ENVIRONMENT & HEALTH

Open Access

pubs.acs.org/EnvHealth

Article

The Opposite Roles of Benzo[*a*]pyrene Eco-Corona and Bronchoalveolar Lavage Fluid Biocorona in the Cytotoxicity of Polystyrene Microplastics

Published as part of Environment & Health special issue "Micro- and Nano-plastics: What's Hidden Beneath".

Rui Hou, Ye-xuan Zhang, Si-si Chen, Sen Zhang, Li Mao,* Hong-juan Chen, Yong Wang, Wei-juan Zheng, Hong-wei Wang, and Hong-zhen Lian*

Cite This: *Environ. Health* 2026, 4, 1567−1580

Read Online

ACCESS | Metrics & More | Article Recommendations | Supporting Information

ABSTRACT: Microplastics (MPs) have recently become a worldwide concern as newly emerging airborne pollutants, particularly because they can associate with polycyclic aromatic hydrocarbons (PAHs). Upon inhalation, MPs encounter bronchoalveolar lavage fluid (BALF), resulting in the formation of protein coronas that govern their biological identity and behavior. Herein, polystyrene (PS) MPs were selected as model MPs, and PS@BALF, PS@BaP, and PS@BaP@BALF MPs were simultaneously prepared to study the combined effects of eco- and biocorona formation for the first time. We investigated the compositions of protein coronas formed on PS and PS@BaP MPs in BALF, revealing that BaP adsorption significantly altered protein species and relative abundance. It was found that the protein corona enhanced uptake of PS MPs by RAW264.7 macrophages through caveolin-mediated endocytosis, with SP-A identified as a key mediator. Moreover, cytotoxicity assessments demonstrated that the protein corona mitigated membrane damage and apoptosis induced by MPs, whereas BaP adsorption significantly intensified cellular toxicity, oxidative stress, and apoptotic responses, illustrating the opposing effects of two coronas. Notably, the protein corona contributed to oxidative stress, potentially due to increased cellular uptake. Finally, toxicoproteomics analysis elucidated potential mechanisms of MP-induced toxicity. These findings underscore the importance of incorporating both pollutant adsorption and biomolecular corona formation.

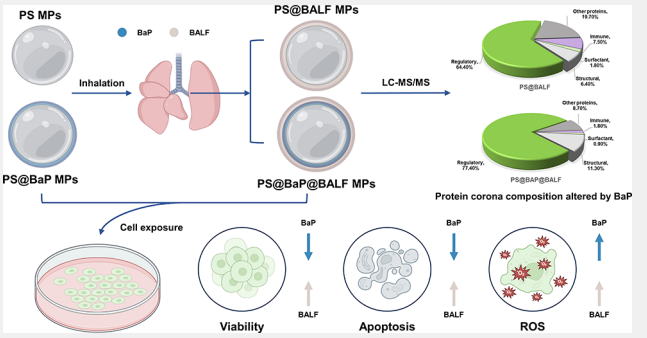

KEYWORDS: *Polystyrene microplastic, Bronchoalveolar lavage fluid, Benzo[a]pyrene, Corona, Combined cytotoxicity, Proteomics*

1. INTRODUCTION

Plastics are ubiquitous in daily life, representing one of the fastest-growing and most widely produced materials worldwide.[1−3] As of 2020, global plastic production had reached 500 million tons, and it is projected to double by 2050, exceeding 1 billion tons annually, with a cumulative output estimated at 33 billion tons.[4] Currently, only about 9% of plastic waste is recycled,[2] while 74%−94% ends up in landfills, incinerators, or the natural environment,[4] leading to persistent environmental contamination. In the environment, plastics undergo aging and fragmentation, generating smaller particles known as microplastics (MPs).[5,6] MPs are commonly defined as plastic particles smaller than 5 mm, with 0.1 μm considered the lower boundary,[7,8] and are categorized as either primary or secondary based on their origin.[9] MPs can migrate easily in the environment and enter the human body via ingestion, inhalation, or skin contact due to the small size.[10] Previous research have confirmed their presence in various human organs, including the liver, kidney, and lung,[11] and smaller MPs can even penetrate biological barriers and be found in blood,[12] placenta,[13] and brain tissues,[14] raising serious concerns about their potential health effects. However, most research on the health risks of MPs just focused on their impact on the digestive system via ingestion,[15−17] with limited attention to the effects of inhaled MPs on the respiratory system. MPs that enter the body via inhalation can reach the alveoli and may be more difficult to eliminate compared to ingested MPs.[18] Therefore, research on inhaled MPs should not be overlooked. Existing studies have reported the presence of MPs in bronchoalveolar lavage fluid (BALF),[18] human sputum,[19] lower respiratory tract samples[20,21] and lung tissue,[22] with an average concentration of approximately 9 particles per 100 mL

Received: December 10, 2025
Revised: April 9, 2026
Accepted: April 12, 2026
Published: April 20, 2026

https://doi.org/10.1021/envhealth.5c00747
Environ. Health 2026, 4, 1567−1580

of BALF.[23] Pulmonary exposure to MPs has been shown to induce toxic effects, including oxidative stress in alveolar epithelial cells,[24] pulmonary fibrosis,[25] and induced hematological system injury.[26]

MPs can interact with other substances through hydrophobic or electrostatic interactions, forming surface-bound layers collectively referred to as corona.[27] Coronas are generally classified into eco-coronas and biocoronas depending on the settling circumstances.[28] The eco-coronas are generated from abiotic environmental media (e.g., metal ions, inorganic anions, and organic chemicals), whereas the biocoronas are acquired from biological fluids (e.g., proteins, lipids, nucleic acids) within living organisms.[4] The formation of coronas can significantly influence the biodistribution and ultimate fate of MPs within the body.[29,30] Due to their small size, high specific surface area, amorphous structure, hydrophobicity, and porosity, MPs readily adsorb hydrophobic environmental contaminants,[31,32] particularly persistent organic pollutants (POPs),[33] such as polycyclic aromatic hydrocarbons (PAHs). Studies have shown that MPs can adsorb PAHs to form eco-coronas.[34,35] Benzo[*a*]pyrene (BaP), a representative PAH, is often used as a marker compound in environmental toxicology.[36] Feng et al.[37] reported that polystyrene (PS) possessed the highest capacity of adsorbing BaP via forming sandwiched π-stacking structures with benzene rings among five nanoplastics (polyvinyl chloride, polyethylene, polypropylene, polyethylene terephthalate, and PS). When adsorbed onto the surface of MPs, BaP can alter their biological effects. For instance, González-Soto et al.[38] reported that PS MPs loaded with BaP exerted greater toxicity in *Mytilus galloprovincialis*, as indicated by reduced hemocyte viability, altered catalase activity, and epithelial damage in digestive tubules, compared to pristine MPs. Similarly, von Hellfeld et al.[39] found that PS MPs adsorbing cadmium or BaP induced histological changes in the digestive glands of *Mytilus galloprovincialis*, whereas pristine MPs had negligible effects after 3 days of exposure. Despite these findings, there is a notable lack of research on the combined toxicological effects of MPs and environmental contaminants on human health, particularly through inhalation routes.[40,41]

Bronchoalveolar lavage fluid (BALF) serves as an ideal model to simulate the pulmonary lining fluid interface encountered by MPs in the lungs following inhalation.[42] Once inhaled, MPs diffuse through the alveolar lining fluid layer containing proteins, lipids, and other components,[43] during which they can adsorb proteins from BALF to form biocoronas. It is essential to explore the formation of protein coronas on MPs in real biological fluids for understanding the implications of human exposure to MPs. However, very few studies have investigated the formation of BALF-derived protein coronas on MPs, with most focusing on engineered nanoparticles rather than MPs. Poulsen et al.[44] examined the composition and concentration of BALF proteins adsorbed onto TiO_2 nanoparticles and reported increased secretion of interleukin-6 (IL-6), tumor necrosis factor-α (TNF-α), and macrophage inflammatory protein-2 (MIP-2). Xia et al.[45] indicated the differences in biocoronas formation on iron oxide nanoparticles incubated in BALF from healthy and metabolically syndrome-affected mice, demonstrating alterations in cellular interactions and toxicity. Shaw et al.[46] found that protein coronas formed on carbon black nanoparticles in BALF enhanced particle phagocytosis 5-fold compared to those formed in plasma or fibrinogen. Only a few studies have analyzed the composition of protein coronas formed on particles after incubation with BALF, as well as their impact on cellular phagocytosis.[47,48] Furthermore, MPs coated with eco-coronas more accurately represent environmental exposures. Notably, BaP may influence the adsorption of BALF proteins onto MPs, thereby altering downstream cellular responses. The impact of protein coronas on combined toxicity, particularly in relation to cell-level toxicological outcomes, remains a critical knowledge gap that warrants further investigation.

PS is widely detected in both indoor and outdoor airborne environments due to its prevalence in common consumer products, such as packaging and textiles.[49−51] As a significant contributor to airborne MPs, PS can adsorb BaP coexisting in the atmosphere, forming a representative combined contaminant that poses potential risks to the respiratory system.[41] Additionally, PS has been commonly employed in MP toxicity studies,[31,33] making it an ideal model for investigating the toxicity mechanisms of MP-pollutant complexes. Herein, we designed a novel protocol to delve into the biological effects and potential toxic mechanisms of PS MPs under in vitro conditions. First, to investigate the initial biological interactions upon inhalation, BaP was preadsorbed onto PS MPs to form eco-coronas-modified MPs, while BALF was used to form biocoronas that mimic the first biological barrier encountered in the alveoli on PS and PS@BaP MPs. The surface properties of different MPs were characterized, and the compositions of the protein coronas adsorbed on PS and PS@BaP MPs were analyzed using SDS-PAGE and LC−MS/MS. Furthermore, toxicological measurements were conducted using RAW264.7 macrophages to compare cytotoxicity, oxidative stress, and apoptosis across the four MP groups, and to assess the effect of protein coronas on cell uptake. In addition, Pro DIA-based quantitative proteomic analysis was performed to identify differentially expressed proteins (DEPs) and enriched pathways in exposed cells, providing more clues to elucidate the toxicity mechanism of MPs−coronas complex.

2. MATERIALS AND METHODS

2.1. Chemicals and Reagents

PS (0.2−0.5 μm, 2.5% w/v) and BaP were purchased from Aladdin (Shanghai, China); 10% chloroform solution was purchased from NJDULY (Shanghai, China); green fluorescent PS was purchased from Baseline (Tianjin, China); physiological saline (0.9%), SDS-PAGE loading buffer (5×), Coomassie Brilliant Blue staining solution, Tris-HCl (1.5 mol/L, pH 8.8), Tris-HCl (1 mol/L, pH 6.8), dimethyl sulfoxide (DMSO), TBSTw (10×), Reactive Oxygen Species (ROS) Detection Kit, BCA protein concentration detection kit, Lactate Dehydrogenase (LDH) Detection Kit, Total Superoxide Dismutase (SOD) Activity Assay Kit (WST-8 method), BeyoECL Moon Detection Kit, RIPA cell lysis buffer, and protease and phosphatase inhibitor mix were purchased from Beyotime Biotechnology (Shanghai, China); phosphate-buffered saline (PBS) and fetal bovine serum (FBS) were purchased from Gibco (USA); Cell Counting Kit-8 (CCK-8 Kit) was purchased from UElandy (Jiangsu, China); CheKine Reduced Glutathione (GSH) Colorimetric Assay Kit was purchased from Abbkine (Wuhan, China); chlorpromazine (CPZ) and 5-(*N*-ethyl-*N*-isopropyl)-aminopyridine (EIPA) were purchased from MCE (Nanjing, China); methyl-β-cyclodextrin (MβCD) was purchased from Sigma-Aldrich (Shanghai, China); Mouse IL-6 ELISA Kit was purchased from ExCell Bio (Jiangsu, China); Annexin V-FITC/PI Apoptosis Detection Kit and high-glucose Dulbecco's modified Eagle medium (DMEM) containing 1% penicillin and streptomycin were purchased from KeyGEN BioTECH (Jiangsu, China); MAP4K3 polyclonal antibody (rabbit polyclonal), alpha-tubulin antibody (rabbit polyclonal) were purchased from Proteintech

https://doi.org/10.1021/envhealth.5c00747
Environ. Health 2026, 4, 1567−1580

(USA); fibrinogen α-chain antibody (rabbit monoclonal) and horseradish peroxidase-labeled goat antimouse IgG (H+L) were purchased from Abcam (Shanghai, China). BALF was obtained by ten healthy SPF SD rats aged 9−11 weeks and weighing 300−330 g. Rats were anesthetized with 10% chloral hydrate, and the trachea was exposed. The lungs were lavaged three times with 6 mL of physiological saline and slowly aspirated back and forth each time. Then the BALF samples were centrifuged at 1500 r/min for 10 min at 4 °C to pellet large agglomerates and cellular debris. All supernatant samples were pooled into a homogeneous solution and stored at −80 °C to avoid protein degradation. The concentration of BALF was determined using BCA Protein Assay Kit. The animal experiments were approved by the Animal Research Committee of Nanjing University Medical School (2024-AE01082).

2.2. Preparation of PS@BALF MPs

PS MPs (1 mg/mL, 1 mL) were incubated with 3 mL of BALF at 37 °C for 1 h. The concentration of MPs used for characterization was selected based on previous studies.[45,52,53] After that, the suspensions were centrifuged at 16,000 × *g* at 4 °C for 30 min, followed by washing three times with 1 mL of precooled physiological saline to remove unadsorbed protein. The prepared PS@BALF MPs were resuspended in ultrapure water or DMEM for subsequent experiments.

2.3. Preparation of PS@BaP and PS@BaP@BALF MPs

BaP solutions with the concentrations of 0.01, 0.05, 0.2, 0.5, 1, and 2 μg/mL were prepared by gradient dilution with 100 μg/mL of BaP solution. PS MPs (1 mg/mL, 1 mL) were incubated with 0.1 mL of the above different concentrations of BaP at 25 °C for 24 h, then the suspensions were centrifuged at 16,000 × *g* at 4 °C for 30 min, followed by washing three times with 1 mL of ultrapure water to remove unadsorbed BaP to obtain PS@BaP MPs for characterization. 1 mL of acetonitrile (ACN) was added to elute the PS@BaP MPs, followed by vortex sonication for 1 h and incubation at room temperature for 24 h. Then the suspensions were centrifuged at 16,000 × *g* at 4 °C for 30 min and the fluorescence signal of BaP was detected by fluorescence spectrometry (FL) (F-7000, Hitachi, Japan). PS@BaP@BALF MPs were obtained by the same methods as those used for PS@BALF MPs. The MPs were resuspended in ultrapure water or DMEM for subsequent experiments.

2.4. Characterization of the MPs

The size and morphology of the MPs were characterized by a scanning electron microscopy-energy dispersive X-ray spectroscopy (SEM-EDX) (S-4800, Hitachi, Japan), and the functional groups on the surface and chemical compositions of the MPs were analyzed by an attenuated total reflection Fourier transform infrared (ATR-FTIR) spectrometer (Nicolet iS10, ThermoFisher Scientific, USA). The hydrodynamic diameters of the MPs in ultrapure water and DMEM medium were measured using a dynamic light scattering (DLS) (90 Plus, Brookhaven, USA), and the zeta potential of the MPs in ultrapure water and DMEM was determined by a zetasizer (Nano-Z, Malvern, UK).

2.5. Characterization of Protein Corona Compositions

The proteins adsorbed on the surface of PS@BALF and PS@BaP@BALF MPs were eluted according to previous literature.[54] For SDS-PAGE analysis, bands were observed to confirm the presence of protein coronas. Then the compositions of the protein coronas were analyzed using liquid chromatography−mass spectrometry/mass spectrometry (LC−MS/MS) (TripleTOF 5600+AB Sciex, USA). Details are described in Supplementary Text S1.1.

2.6. Cell Culture

Mouse macrophage RAW264.7 cells were cultured in high glucose DMEM that contains 10% (v/v) FBS in a saturated humidified 5% CO_2 atmosphere at 37 °C for incubation.

2.7. Endocytosis Determination

Cells in logarithmic growth phase were seeded on 6-well plates at a density of 5 × 10^4 cells/well, with 2 mL per well. After being incubated at 37 °C for 24 h, cells were pretreated with CPZ (3 μg/mL), MβCD (5 mg/mL), and EIPA (50 μmol/L) for 30 min, respectively. Then the cells were incubated with green fluorescent PS, PS@BALF, PS@SPA MPs (150 μg/mL) for 4 h. The concentrations of MPs and endocytosis inhibitors were selected based on previous studies,[41] and also on cytotoxicity results. The wells without endocytosis inhibitors were used as the control group. After that, the cells were washed three times with precooled PBS and centrifuged at 1,000 × *g* at 4 °C for 5 min. The fluorescence signals of internalized MPs were detected using a flow cytometer (Cytomics FC 500, Beckman Coulter, USA).

2.8. Cell Viability

Cell viability of RAW264.7 cells after exposure to PS, PS@BALF, PS@BaP, and PS@BaP@BALF MPs for 24/48 h was determined by CCK-8. Details are described in Supplementary Text S1.2. The concentrations of different MPs used for all cell stimulation experiments were selected based on previous studies.[41,48,53,55]

2.9. LDH Release Measurement

LDH content in the culture medium of RAW264.7 cells after exposure to PS, PS@BALF, PS@BaP, and PS@BaP@BALF MPs for 24/48 h was determined using the LDH assay kit. Details are described in Supplementary Text S1.3.

2.10. Cell Apoptosis

The cell apoptosis rate of RAW264.7 cells after exposure to PS, PS@BALF, PS@BaP, and PS@BaP@BALF MPs for 24/48 h was analyzed using the apoptosis detection kit. Details are described in Supplementary Text S1.4.

2.11. Intracellular ROS Measurement

Intracellular ROS levels of RAW264.7 cells after exposure to PS, PS@BALF, PS@BaP, and PS@BaP@BALF MPs for 24 h were measured. Details are described in Supplementary Text S1.5.

2.12. Measurements of SOD Activity and GSH Content

SOD activity and GSH content of RAW264.7 cells after exposure to PS, PS@BALF, PS@BaP, and PS@BaP@BALF MPs for 24 h were assessed. Details are described in Supplementary Texts S1.6−1.8.

2.13. Proteomics

To analyze the protein expression levels, lysates of RAW264.7 cells after exposure to PS, PS@BALF, PS@BaP, and PS@BaP@BALF MPs (150 μg/mL) for 24 h were prepared and the proteins were extracted, trypsin digested, and peptide desalted. Finally, the processed samples were analyzed by EASY-nLC 1200 liquid chromatography (ThermoFisher, USA) and timsTOF Pro (Bruker, Germany). Details are described in Supplementary Text S1.9.

2.14. Detection of IL-6 Protein Level

The concentration of IL-6 in the culture medium of RAW264.7 cells after exposure to PS, PS@BALF, PS@BaP, and PS@BaP@BALF MPs for 24 h was determined by enzyme-linked immunosorbent assay (ELISA) using the Mouse IL-6 ELISA Kit (Excell, China). Details are described in Supplementary Text S1.10.

2.15. Western Blot Analysis

After exposure to PS, PS@BALF, PS@BaP, and PS@BaP@BALF MPs for 24 h, RAW264.7 cells were lysed in RIPA cell lysis buffer. The lysates were run on gels and immunoblotted with relevant antibodies using standard methods.[54] Details are described in Supplementary Text S1.11.

2.16. Statistics and Bioinformatics

All the measurements were repeated at least three times. The results were expressed as means ± standard deviations (SD). One-way analysis of variance (ANOVA) was employed to analyze statistical significances of differences in multiple groups, where *: $p < 0.05$, **: $p < 0.01$, ***: $p < 0.001$, ****: $p < 0.0001$. The LC−MS/MS data processing in label-free and Pro DIA proteomics were described in Supplementary Text S1.12.

https://doi.org/10.1021/envhealth.5c00747
Environ. Health 2026, 4, 1567−1580

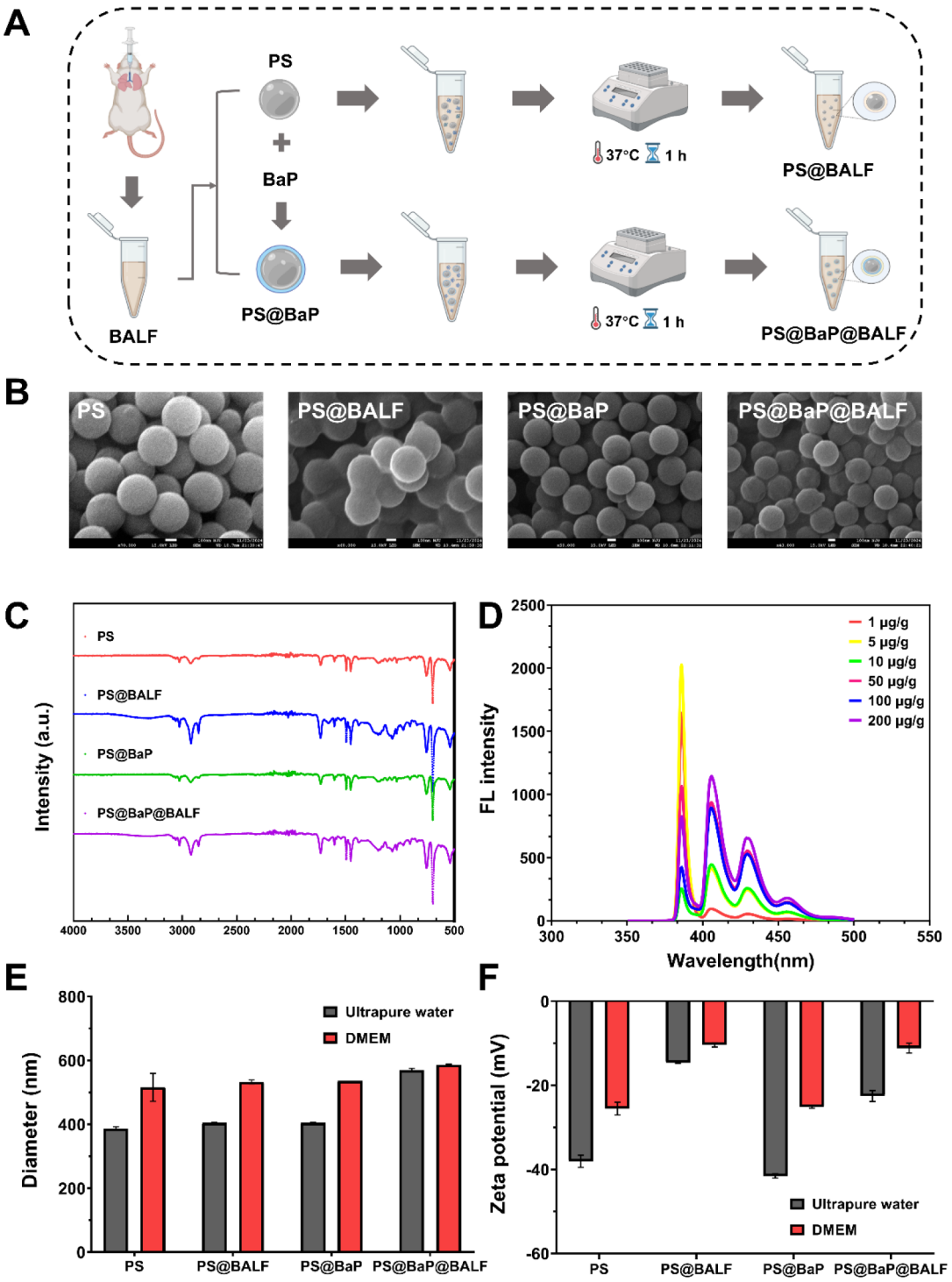

Figure 1. Scheme of the preparation procedures of PS@BALF, PS@BaP, and PS@BaP@BALF MPs (A). SEM images (B), ATR-FTIR spectra (C), hydrodynamic dimensions (E), and zeta potentials (F) of PS, PS@BALF, PS@BaP, and PS@BaP@BALF MPs. Adsorption of BaP on PS MPs (D).

3. RESULTS AND DISCUSSIONS

3.1. Coronas Altered the Physicochemical Characteristics of PS MPs

The small size, high surface area of MPs, in combination with the hydrophobicity, make them highly reactive toward atmospheric PAHs such as BaP, conferring new biological properties on MPs. As is considered to be one of the most widely used plastics, PS MPs were selected as the representative model in this study.[56] To simulate the progress, both pristine and BaP-adsorbed PS MPs were incubated with BALF upon inhalation, with the formation of protein coronas (Figure 1A). As illustrated in the SEM images (Figure 1B), the morphologies and structures of the MPs were observed. The average sizes of different MPs were statistically analyzed (Figure S1). PS MPs exhibited a spherical shape with uniform size, with an average particle size of 348.5 nm. A membrane-like structure was observed on PS@BaP MPs, which maintained a monodisperse state with an average particle size of 365.9 nm. The entire surfaces of PS and PS@BaP MPs

https://doi.org/10.1021/envhealth.5c00747
Environ. Health 2026, 4, 1567−1580

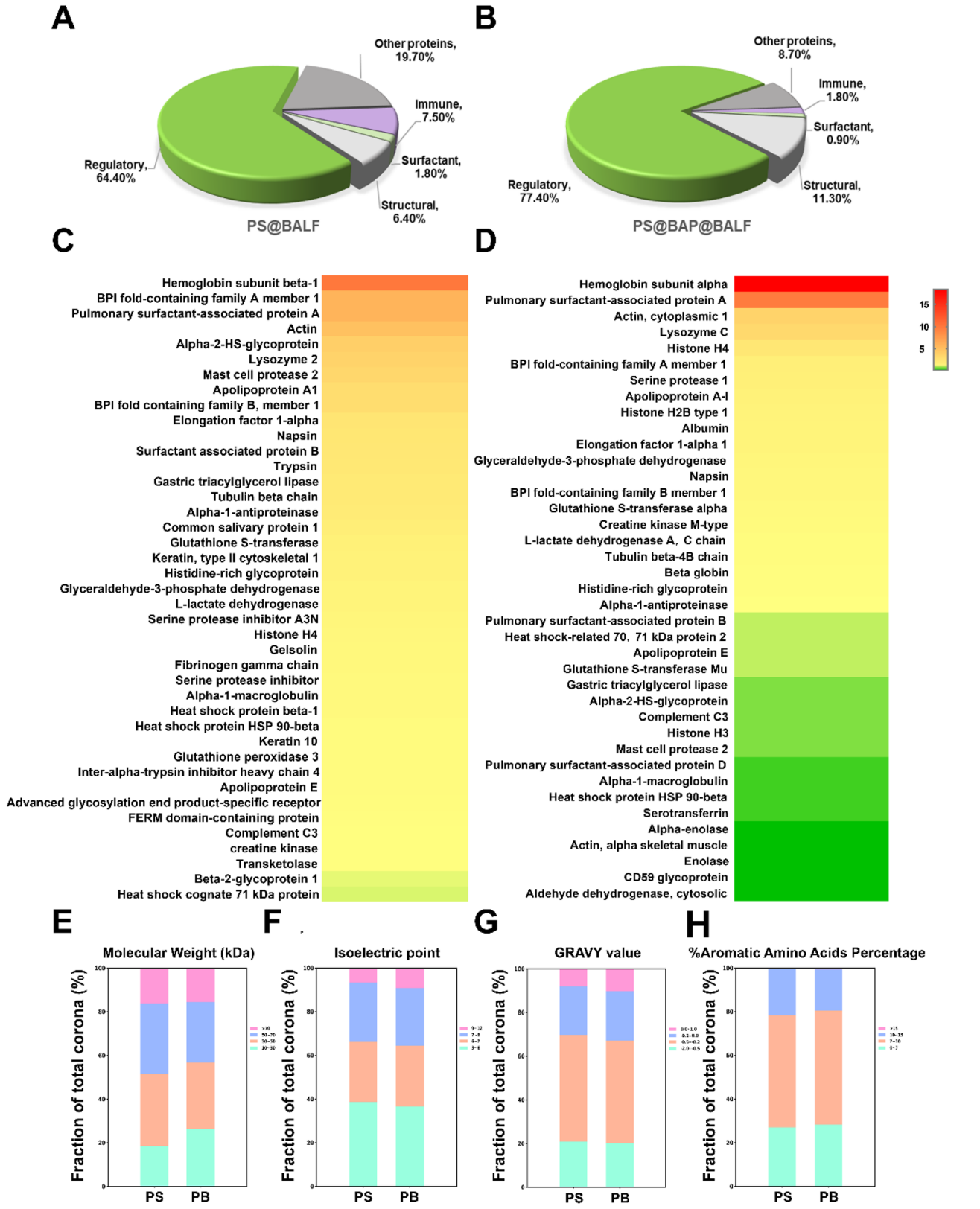

Figure 2. Classification of identified proteins on PS and PS@BaP MPs according to their biological functions (A, B). The proteins with a protein content (mol %) greater than 0.6% in BALF coronas on PS MPs (C). The proteins with a protein content (mol %) greater than 0.2% in BALF coronas on PS@BaP MPs (D). Molecular weight (E), isoelectric point (F), GRAVY value (G) and % aromatic amino acids (H) of proteins in BALF coronas on PS and PS@BaP (PB) MPs.

were coated with protein coronas practically after incubation with BALF, and the average particle sizes of PS@BALF and PS@BaP@BALF MPs were 382.2 and 383.9 nm, respectively. Additionally, elemental mapping by EDX revealed the presence

https://doi.org/10.1021/envhealth.5c00747
Environ. Health 2026, 4, 1567−1580

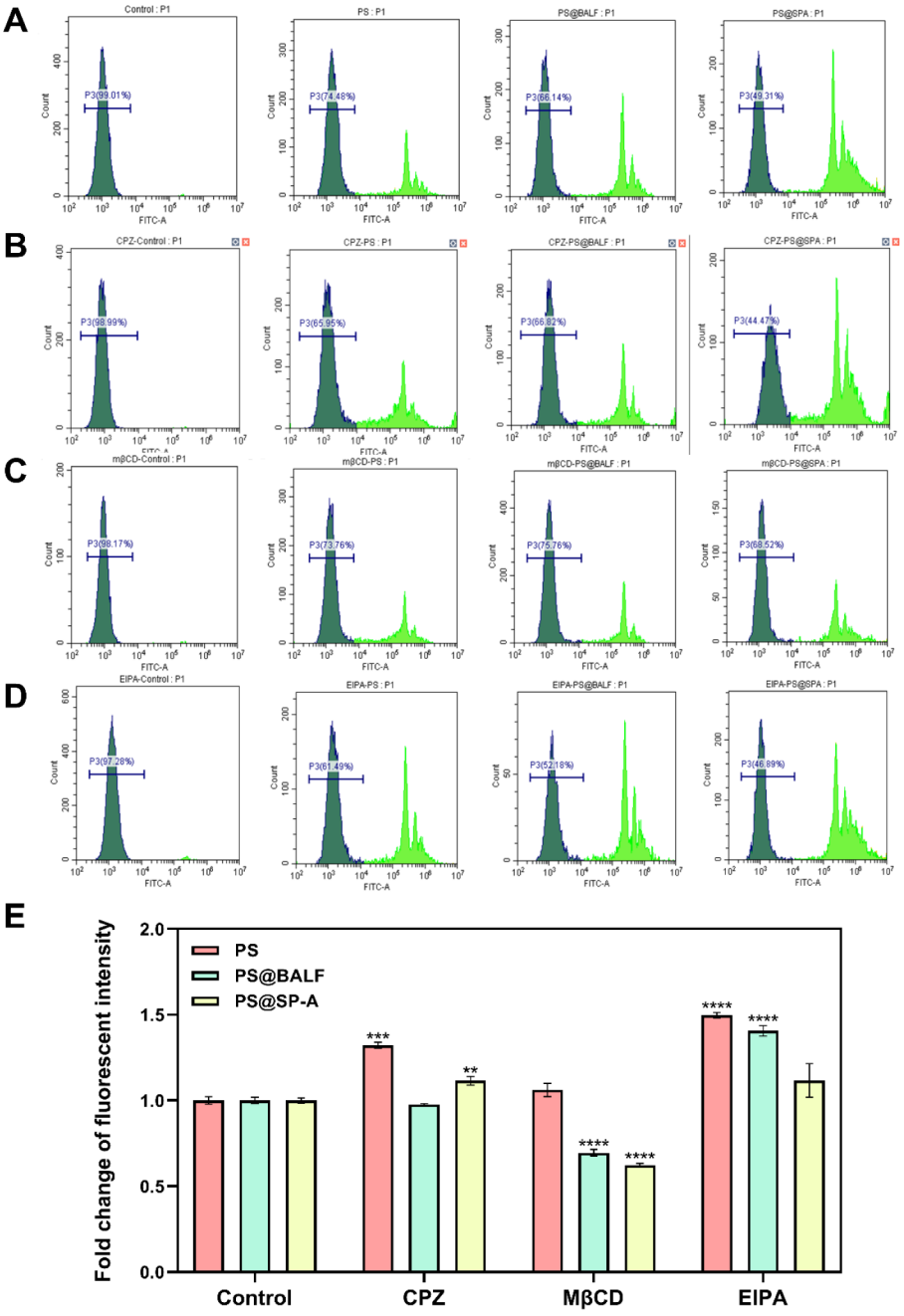

Figure 3. RAW264.7 cells were exposed to PS, PS@BALF, and PS@SP-A for 24 h. The uptake of MPs by RAW264.7 cells was determined by flow cytometry (A). Effects of CPZ (B), MβCD (C), EIPA (D) on uptake of PS, PS@BALF, and PS@SP-A MPs (150 μg/mL) in RAW264.7 cells after incubation for 4 h. The fluorescent intensity changes were normalized to the mean fluorescent intensity of controls (E).

of protein-specific elements (O, S, P) on the surface of PS@BALF MPs (Figure S2). Previous studies support the results as they reported the formation of protein coronas on PS particles, and the observation of the coronas feature.[41,48]

The functional groups on the MPs also changed obviously upon adsorbing BALF as showed in Figure 1C. The FTIR spectra of PS@BaP MPs was similar to pristine PS MPs, due to the similar functional groups and elemental compositions, showing the characteristic peaks of C−H stretching vibration of the aromatic ring at 3063 and 3026 cm^{-1}, C−H_2 stretching vibration of the main chain at 2922 and 2852 cm^{-1}, C═C stretching vibration of the aromatic ring at 1601, 1492, and 1452 cm^{-1} and C−H bending vibration of the aromatic ring at 754 and 697 cm^{-1}. In contrast, three distant peaks at 3316, 1654, 1542 cm^{-1} were observed after BALF adsorption, which corresponded to N−H stretching vibration, C═O stretching vibration, C−N stretching vibration and N−H bending in −CO−NH−, respectively.[41]

As shown in Figure 1D, fluorescence spectroscopy was employed to quantify BaP adsorption on PS MPs at six theoretical adsorption concentrations (BaP/PS = 1, 5, 10, 50, 100, and 200 μg/g). Based on the previous study, the adsorption capacity of PAHs on MPs ranged from 46 to 236 μg/g.[57] The standard curve was shown in Figure S3. We found that the actual adsorption concentration plateaued at 20 μg/g

https://doi.org/10.1021/envhealth.5c00747
Environ. Health 2026, 4, 1567−1580

when the theoretical adsorption concentration reached 50 μg/g, with an adsorption rate of 42.6% (Table S1).

The hydrodynamic diameters and zeta potentials of the MPs were further measured. As shown in Figure 1E, the hydrodynamic diameters of PS, PS@BALF, PS@BaP and PS@BaP@BALF MPs in ultrapure water/DMEM medium were 386.7/470.7, 404.5/538.3, 404.6/535.8 and 574.5/585.6 nm, respectively. The larger size of PS@BaP MPs may be due to increased surface roughness. Meanwhile, the formation of protein coronas enhanced the hydrophilicity and increased the thickness of the hydrated layer. The observed differences in DMEM medium may be attributed to the presence of amino acids, salts, and other components. Similarly, Zhou et al.[58] reported that the hydrodynamic diameters of $PM_{2.5}$ particles in ultrapure water were smaller than in simulated lung fluid, likely due to the effect of ions in the buffer. The zeta potentials of PS, PS@BALF, PS@BaP and PS@BaP@BALF MPs in ultrapure water/DMEM medium were −38.0/−25.5, −14.6/−10.4, −41.6/−25.1 and −41.2/−11.1 mV, respectively (Figure 1F). It suggested that adsorption of BaP led to a slight increase in electrostatic stability, while protein coronas reduced the electrostatic stabilization of MPs. These results were consistent with previous findings explaining that particle stability is altered by adsorbed proteins, changing the hydrophilicity and interfacial charge.[54]

3.2. BaP Influenced the Protein Coronas on PS MPs Formed in BALF

Previous studies have reported the coronas formation on bare PS MPs, but there is limited research on how the adsorption of other environmental contaminants, such as BaP, affects protein corona formation, particularly in BALF. As the coronas may modulate the biokinetics of MPs, we examined the composition of the protein coronas on MPs after BALF incubation. SDS-PAGE and total protein staining were conducted to visualize the coronas on MPs (Figure S4). As the concentration of PS MPs increased, more protein bands appeared, however, no significant differences in protein abundance or diversity were observed between PS and PS@BaP MPs. Immediately, we performed LC−MS/MS to specifically analyze the compositions of coronas on PS and PS@BaP MPs (Tables S3 and S4). Albumin, lysozyme, and hemoglobin were identified as the major proteins in BALF, suggesting inevitable blood cell contamination during BAL (Figure S5). As shown in the Venn diagram (Figure S6), a total of 149 and 273 proteins were identified in the coronas on PS and PS@BaP MPs, respectively, with 73 and 197 distinct proteins on the two MPs, respectively. This indicated that BaP adsorption led to a wider variety of protein adsorption, thus resulting in the increased hydrophobicity and protein adsorption capability of MPs.

Moreover, the identified proteins were then categorized based on their biological functions (Figure 2A,B), including immune-related proteins (e.g., complement C3, C4), surfactant proteins (e.g., SP-A, SP-B), structural proteins (e.g., fibrinogen α, γ) and regulatory proteins (e.g., apolipoprotein A, E). Regulatory proteins were the most abundant category on PS MPs (64%), increasing by 13% after BaP adsorption. Apolipoproteins, one of the regulatory proteins, are involved in lipid transport and can regulate cellular uptake by binding to specific cell surface receptors, as reported for ApoA.[59]

The further highlighted differences in major protein species were shown in detail by heatmaps (Figure 2C,D). In both groups, proteins such as hemoglobin, SP-A, ApoA-I, and albumin were highly enriched. These selectively adsorbed proteins have important physiological functions that may alter cellular responses. SP-A, in particular, was the dominant protein in both coronas. SP-A could be bound onto the surface of particles upon BALF exposure.[60] As an important innate immune molecule in lung surfactants, SP-A can facilitate phagocytosis of inhaled particles.[61,62]

In addition, the biochemical properties of the proteins in BALF coronas on PS and PS@BaP MPs, including molecular weight, isoelectric point, GRAVY value, and aromatic amino acid content, were investigated by abundance weighting (Figure 2E−H).[59] The aromatic amino acids of proteins bound to PS and PS@BaP MPs were essentially unchanged. However, PS@BaP MPs adsorbed smaller molecular weight proteins, binding proteins with relatively higher isoelectric points and more positive GRAVY values. Thus, the results suggested that PS MPs tend to adsorb more positively charged hydrophilic proteins after BaP adsorption, possibly due to increased surface hydrophobicity. Therefore, the potential biological effects of these selectively adsorbed proteins on BaP-adsorbed PS MPs may be overlooked in studies performing pristine MPs. In general, our findings provide valuable clues for further studies on the effect of surface modification of MPs on protein coronas formation.

3.3. BALF Coronas Affected the Cellular Uptake of PS MPs

The formation of protein coronas after BALF incubation remarkably altered the cellular adhesion of PS MPs and resulted in differences in cellular uptake, so it is necessary to suspect that protein coronas may affect the endocytosis mechanism of cells. The relative fluorescence intensity changes of the flow cytometry FITC channel were used to evaluate the endocytic efficiency of PS MPs after 24 h cell treatment.[63] As shown in Figure 3A, compared with PS MPs, the fluorescence intensity of RAW264.7 cells treated with PS@BALF MPs was increased from 25.52% to 33.86%, which may be attributed to the exposure of new epitopes on the surface of PS MPs when they contact the cell membrane, thereby enhancing particle−cell membrane affinity. Additionally, the composition of the protein coronas also plays a key role in the enhanced cellular uptake.[64] We selected SP-A, a highly abundant protein in BALF coronas, to assess its specific contribution to uptake. PS@SP-A MPs were prepared by incubating purified SP-A protein with PS MPs, revealing a significant increase in uptake (from 25.52% to 50.69% in Figure 3A), indicating that SP-A plays a key role in protein corona-mediated cellular internalization. Similarly, Raesch et al.[65] reported that SP-A adsorption on particle surfaces promoted macrophage phagocytosis of particles. The larger hydrodynamic diameter of PS@SP-A compared to PS and PS@BALF (Figure S7) may reflect a denser or more structured corona formed by SP-A, potentially enhancing cellular uptake.

To further explain the effect of protein coronas on the potential internalization pathways of PS MPs, RAW264.7 cells were pretreated with typical endocytic inhibitors, including CPZ, MβCD, and EIPA, to inhibit clathrin-mediated endocytosis, caveolin-mediated endocytosis, and macropinocytosis, respectively. The concentrations of three inhibitors we adopted were validated, showing no appreciable effect on cell viability (Figure S8). As shown in Figure 3C,E, pretreatment with MβCD resulted in a marked decrease in uptake of PS@BALF and PS@SP-A MPs by 30.5% and 37.8%, respectively,

https://doi.org/10.1021/envhealth.5c00747
Environ. Health 2026, 4, 1567−1580

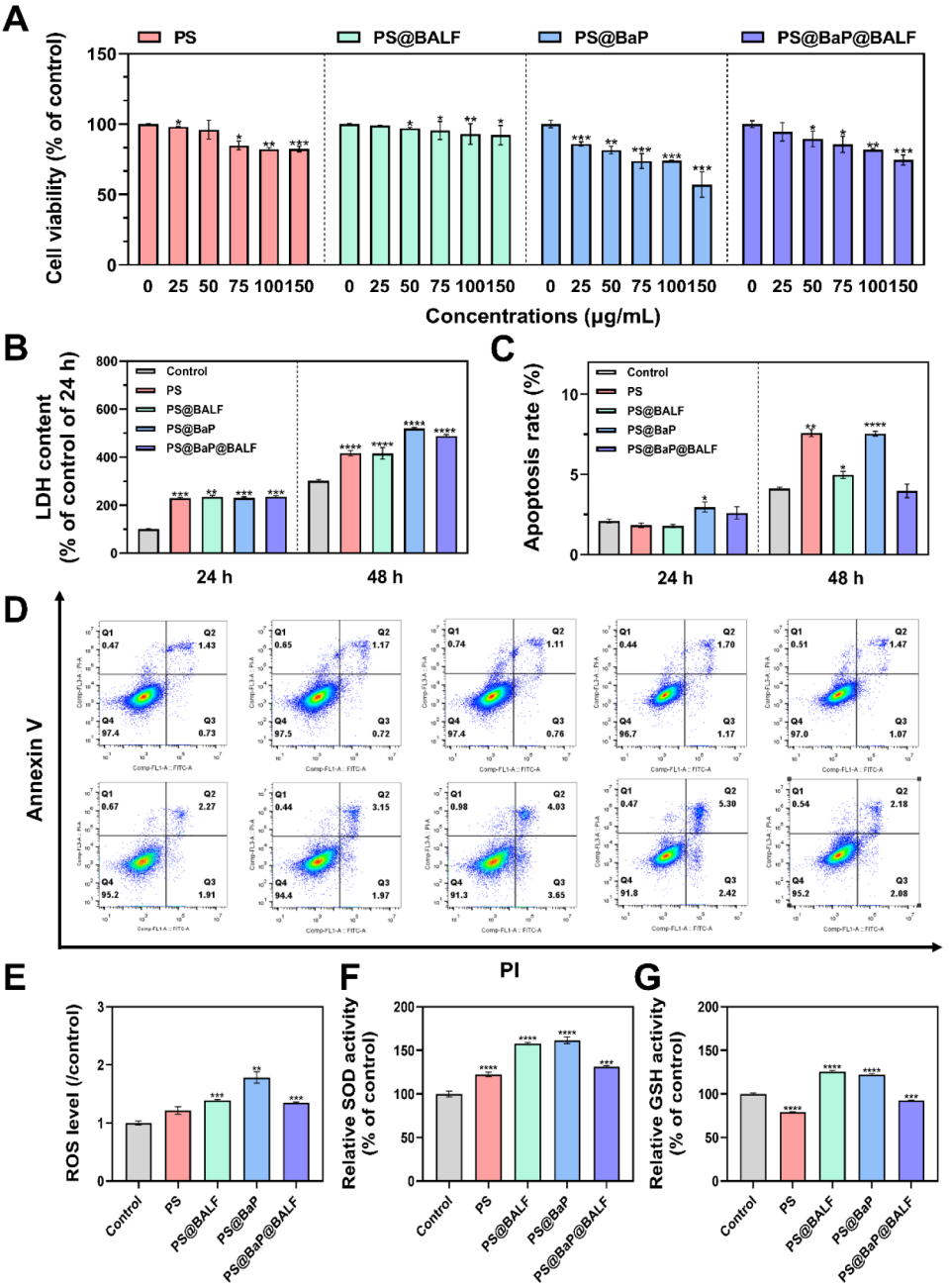

Figure 4. Cell viability of RAW264.7 cells after exposure to PS, PS@BALF, PS@BaP, and PS@BaP@BALF MPs for 48 h (A); LDH content in the culture medium after exposure to MPs for 24 and 48 h (B). Apoptosis rates of RAW264.7 cells after exposure to MPs for 24 and 48 h (C, D). Intracellular ROS levels (E), SOD activity (F), and GSH content (G) in RAW264.7 cells after exposure to MPs for 24 h.

indicating that both were primarily internalized via caveolin-mediated endocytosis. It has been demonstrated that the inhibitory effect of MβCD may diminish due to its mechanism of action via cholesterol depletion when apolipoprotein levels are low, which is tied to apolipoprotein-mediated transport. Notably, pretreatment with CPZ and EIPA (Figure 3B,D) led to a slight increase in cell uptake, possibly due to the inhibition of the primary endocytosis pathway, which subsequently activated compensatory pathways.

In summary, PS@BALF and PS@SP-A MPs were mainly internalized through caveolin-dependent endocytosis, indicating that protein coronas could alter the endocytosis mechanism and enhance cellular internalization of PS MPs, with SP-A playing a dominant role. This SP-A-mediated enhancement can be attributed to its structural and functional properties. Possessing both collagen-like and carbohydrate recognition domains, SP-A acts as a bridging molecule, binding to particulate surfaces and specific receptors on macrophages such as SP-A receptor 210.[66,67] This receptor−ligand interaction is known to initiate intracellular signaling that promotes membrane remodeling and cytoskeletal rearrangement, facilitating the formation and internalization of caveolin. Thus, SP-A not only increased particle recognition but also actively directed them into the caveolin-mediated endocytic pathway, aligning with its physiological role in targeted clearance of inhaled particles from the alveoli.

https://doi.org/10.1021/envhealth.5c00747
Environ. Health 2026, 4, 1567−1580

3.4. Integrated Toxicity Evaluation of Coronas on MPs in RAW264.7 Cells

The cytotoxicities of PS, PS@BALF, PS@BaP, and PS@BaP@BALF MPs to RAW264.7 cells were assessed using CCK-8 assay. As shown in Figure S9, after 24 h stimulation, PS MPs resulted in a slight 5% decline in cell viability within the concentration range of 0−50 μg/mL. When the concentration was increased to 100−150 μg/mL, cell viability decreased by approximately 15%, indicative of concentration dependence. However, the cytotoxicities of PS@BALF, PS@BaP, and PS@BaP@BALF MPs were unstable, with no obvious patterns observed. This may reflect the cells' adaptive response to external stimuli and the regulation of the cell cycle in RAW264.7 cells under serum-free conditions. When the exposure time was extended to 48 h, the cytotoxicity of different MPs showed a clearer concentration-dependent pattern (Figure 4A). PS MPs exhibited minimal toxicity below 50 μg/mL but caused approximately 20% reduction in cell viability at 75−150 μg/mL. After 48 h of stimulation with PS@BALF MPs, there was only a slight decrease in cell viability, which was significantly higher than that observed for PS MPs following BALF adsorption, suggesting that the BALF coronas reduced the cytotoxicity of PS MPs on RAW264.7 cells. In contrast, PS@BaP MPs led to a marked reduction in viability, with a 32% decrease observed at 150 μg/mL, indicating that BaP adsorption enhanced the toxicity of PS MPs. Interestingly, PS@BaP@BALF MPs exhibited reduced cytotoxicity compared to PS@BaP MPs, again highlighting the protective effect of the BALF coronas. This finding agreed with studies that protein coronas can significantly reduce particle-induced cytotoxicity.[41,53] Moreover, compared with the cell viability induced by BaP alone (Figure S10), PS@BaP MPs elicited greater toxicity than the sum of that caused by PS and BaP individually, suggesting an enhanced toxic response. It is important to note that this enhanced toxicity may be attributed to the role of PS MPs as carriers, which potentially alter the uptake route, intracellular localization, and release kinetics of BaP, thereby increasing its bioavailable fraction within cells. Future studies quantifying intracellular BaP concentrations are warranted to investigate toxic interactions between MPs and pollutants.

LDH release is considered an important indicator of cell membrane integrity and is widely used in cytotoxicity assays.[68] As shown in Figure 4B, LDH release increased over time. After 24 h of stimulation, there were no significant differences among the groups. However, after 48 h of stimulation, differences in LDH release (PS@BaP > PS@BaP@BALF > PS > PS@BALF MPs) were observed, consistent with the trend in viability. This indicated that the BALF protein coronas mitigated membrane damage, whereas BaP exacerbated it.

Apoptosis is generally considered an important factor in the cytotoxicity induced by MPs.[69] Apoptosis was analyzed via Annexin V/PI double staining and flow cytometry. As shown in Figure 4C,D, when exposed for 24 h, neither type of MPs induced significant apoptosis, with rates remaining below 3%. After 48 h of exposure, PS MPs induced a 7.7% apoptosis rate, while PS@BALF MPs induced a rate of 5.1%, representing a 34.4% reduction. Similarly, PS@BaP@BALF MPs (4.3%) induced a 47.4% reduction in apoptosis compared to PS@BaP MPs (7.72%). These results were consistent with cell viability and LDH results. However, as the apoptosis rates remained below 10%, apoptosis may not be the primary cause of cytotoxicity in this study.

MPs-induced oxidative stress in cells is considered an important mechanism of MP toxicity, with ROS serving as a biomarker of oxidative stress. The DCFH-DA probe was utilized to detect intracellular ROS levels, with the results expressed as a fold change relative to the control group, as illustrated in Figure 4E. PS MPs did not significantly elevate ROS levels after 24 h, although flow cytometry scatter plots showed increased SSC values, confirming cellular uptake. In contrast, PS@BALF and PS@BaP MPs significantly increased intracellular ROS, reaching 1.39- and 1.78-fold of the control, respectively. We observed that protein coronas led to elevated ROS production, which may be due to enhanced cellular uptake. The previous report has shown that RAW264.7, as macrophages phagocytosing exogenous particles, produced a large amount of ROS, ultimately leading to cellular damage.[70] Interestingly, PS@BaP@BALF MPs induced 24.2% lower ROS levels than PS@BaP MPs, comparable to the ROS levels induced by PS@BALF MPs. Ji et al.[41] found that BaP can detach from PS in lysosomes, enter the cytoplasm, and trigger ROS overproduction. In contrast, the protein coronas delayed BaP lysosomal recognition and release, thereby reducing ROS generation. It is noteworthy that the presence of BaP engendered a contradictory effect on BALF coronas, with respect to ROS generation.

SOD and GSH are important antioxidant enzymes and antioxidant substances in the body.[71] To further investigate oxidative stress responses, the activity of SOD and the content of GSH in RAW264.7 cells were measured, as shown in Figure 4F,G. It was demonstrated that PS MPs induced higher SOD activity, which was further elevated by BALF and BaP adsorption by 28.9% and 32.1%, respectively. Compared with PS@BaP MPs, SOD activity in RAW264.7 cells exposed to PS@BaP@BALF MPs decreased by 18.7%, consistent with intracellular ROS levels, indicating that SOD activity was activated in RAW264.7 cells after stimulation, thereby resisting and eliminating ROS. Additionally, more GSH content could enhance antioxidant capacity and eliminate excess ROS. As shown in Figure 4G, GSH content was consistent with ROS and SOD results. In summary, the adsorption of BALF and BaP on PS MPs led to massive oxidative stress, but the BALF coronas mitigated this effect when coexisting with BaP.

3.5. Potential Pathways Affected by Different MPs

To elucidate the potential mechanisms underlying the differential cytotoxicity induced by different MPs, we performed toxicological proteomics of RAW264.7 cells exposed to PS, PS@BALF, PS@BaP, and PS@BaP@BALF MPs. A total of 7,008 proteins were identified based on Pro DIA quantitative proteomics. Of these proteins, 86, 226, 287, and 402 DEPs were selected in the PS, PS@BALF, PS@BaP, and PS@BaP@BALF groups, respectively (the details of the DEPs are listed in Tables S5−S8). GO annotations of these DEPs were analyzed (Tables S9−S20), and the respective top 30 significantly enriched GO terms for molecular functions, biological processes, and cellular components were shown in Figures S11−S14. In general, there were a great number of proteins related to immune recognition, protein synthesis, oxidative stress, and cellular metabolism affected by PS, PS@BALF, PS@BaP, and PS@BaP@BALF MPs. The PS MPs group showed enrichment of classic inflammatory pathways such as "canonical NF-kappaB signal transduction" and "positive regulation of tumor necrosis factor production", indicating activation of inflammatory responses, consistent

https://doi.org/10.1021/envhealth.5c00747
Environ. Health 2026, 4, 1567−1580

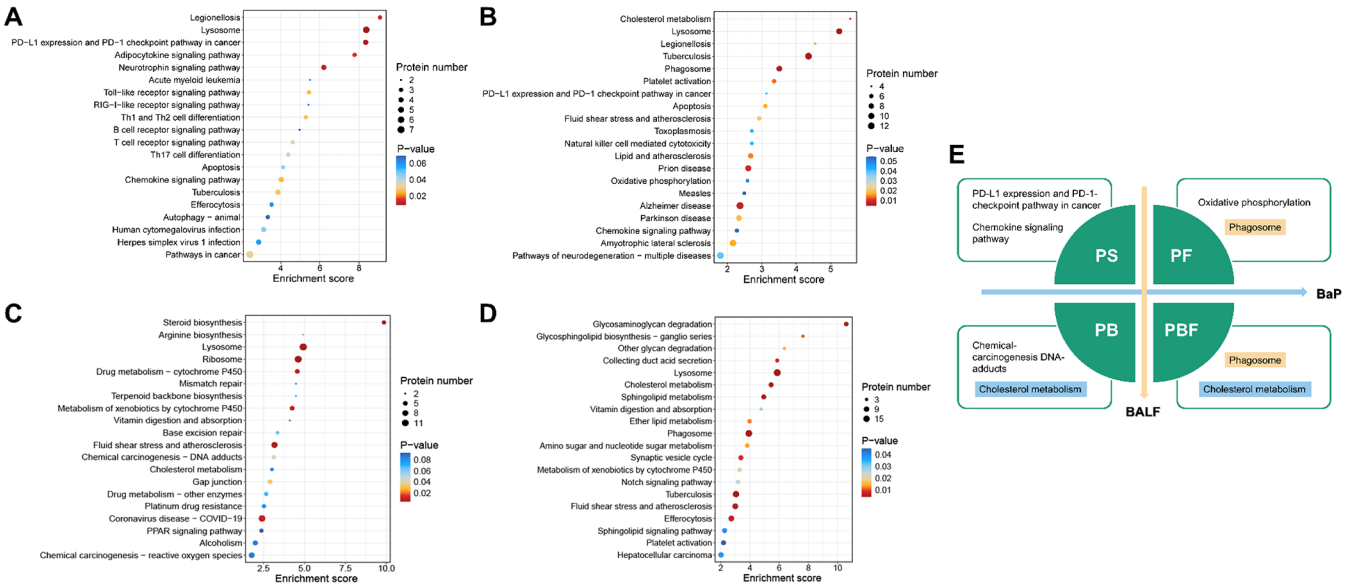

Figure 5. KEGG pathway enriched by DEPs in RAW264.7 cells affected by PS (A), PS@BALF (B), PS@BaP (C) and PS@BaP@BALF (D). The number on the bar is the number of differentially expressed proteins annotated to the pathway, and different colors of the bar represent different KEGG Level information. Schematic diagram of the key signaling pathways affected by PS, PS@BALF (PF), PS@BaP (PB), PS@BaP@BALF (PBF) in RAW264.7 (E).

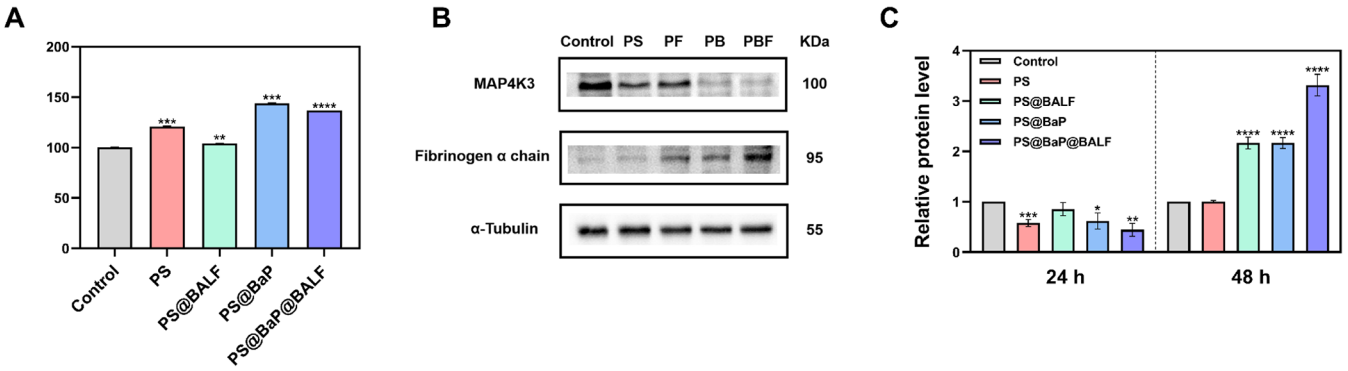

Figure 6. Expressions of MAP3K4 and FGA in RAW264.7 cells after exposed to PS, PS@BALF, PS@BaP, PS@BaP@BALF for 24 h (A, B). IL-6 levels in culture medium of RAW264.7 cells after exposure to MPs for 24 h (C).

with previous findings.[72] The PS@BALF MPs group exhibited concurrent enrichment of the GO terms "negative regulation of neutrophil activation" and "positive regulation of tumor necrosis factor production", suggesting that the protein corona may enhance interactions between MPs and immune recognition elements. Previous studies have reported that macrophages degrade internalized particles through the autophagy−lysosome pathway while regulating inflammatory responses,[73] which is consistent with the enrichment of lysosome-, autophagy-, and vesicle transport-related GO terms observed in the results. In addition, the enrichment of "lipoprotein catabolic process" and "blood microparticle" pathways suggested the role of the BALF protein corona in promoting MPs clearance. In the PS@BaP MPs group, the upregulation of "superoxide dismutase activity" and "glutathione binding" indicated a massive oxidative stress response and enhanced antioxidant defenses. The PS@BaP@BALF MPs group showed enrichment of complex pathways such as "lysosomal protein catabolic process", "lipoprotein catabolic process", and "negative regulation of autophagic cell death", suggesting that its toxicity may result from the combined effects of BaP and BALF within the intracellular environment.

Meanwhile, the KEGG pathways enriched by DEPs in RAW264.7 cells affected by PS, PS@BALF, PS@BaP, and PS@BaP@BALF MPs were analyzed (Figure 5). There is a common pathway of "Lysosome" shared by four groups, indicating that all MPs induced lysosomal responses in RAW264.7 cells. In addition to this common pathway, in RAW264.7 cells exposed to PS MPs, "PD-L1 expression and PD-1 checkpoint pathway in cancer" and "chemokine signaling pathway" pathways were affected, indicating the activation of immune stress and upregulation of inflammatory signaling. As for PS@BALF stimulation, the "oxidative phosphorylation" pathway was enriched by DEPs, which explained why the elevated levels of ROS, SOD, and GSH in RAW264.7 cells were observed. In contrast, DEPs in the PS@BaP group were predominantly enriched in the "chemical carcinogenesis DNA adducts" and "chemical carcinogenesis reactive oxygen species" pathways. It suggested that BaP adsorbed on PS MPs may be metabolized by cytochrome P450 enzymes into reactive intermediates, leading to the activation of NADPH oxidase, excessive ROS generation, and subsequent oxidative DNA damage. The PS@BaP@BALF group showed enrichment in "glycosaminoglycan degradation", "cholesterol metabolism",

https://doi.org/10.1021/envhealth.5c00747
Environ. Health 2026, 4, 1567−1580

and "phagosome" pathways, suggesting altered cellular processing and clearance mechanisms that likely contribute to its mitigated toxicity. Notably, the "phagosome" signaling pathway was enriched by DEPs in RAW264.7 cells affected by PS@BALF and PS@BaP@BALF MPs (Figure 5E). Here, several upregulated proteins, including Toll-like receptor 2 (TLR2), integrin $\alpha5\beta1$ (ITGA5/ITGB1), and the V-type proton ATPase (vATPase) complex, were identified in the KEGG map of this pathway (Figures S15 and S16). TLR2 is a classic pattern recognition receptor that facilitates pathogen recognition and modulates phagosome maturation via its interaction with downstream signaling components.[74] The ITGA5/ITGB1 can mediate cell−particle adhesion and cytoskeletal rearrangement during phagocytosis, enhancing particle uptake by macrophages.[75] The vATPase complex plays a critical role in the acidification of endosomes and lysosomes, which is essential for receptor-mediated endocytosis and subsequent enzymatic degradation.[76] The upregulation of these proteins suggested that the protein corona of BALF may enhance the cellular uptake and intracellular processing of MPs by promoting interaction with membrane receptors, thereby contributing to reduced cytotoxicity. These findings are in agreement with the cytotoxicity results above showing reduced toxicity in BALF-coated MPs, further supporting the protective role of the protein corona.

To validate these proteomic and pathway findings, we next proceeded with ELISA and Western blot experiments. As a key early response cytokine, IL-6 plays a pivotal role in inflammatory signaling and immune activation.[77,78] As shown in Figure 6A, after 24 h of exposure to PS MPs, IL-6 levels increased by 20.8% compared to the control group, indicating immune stress induction. The PS@BALF group exhibited a 13.9% decrease relative to PS alone, suggesting that the protein corona mitigated inflammatory activation. By contrast, PS@BaP exposure led to a significant 43.7% increase in IL-6 levels, emphasizing the strong proinflammatory potential of BaP. In the PS@BaP@BALF group, however, this increase was slightly attenuated by 4.9%, which further confirms that the protein corona can alleviate inflammatory responses. This observation was consistent with the results of KEGG pathway enrichment analysis and cytotoxicity. Furthermore, two representative DEPs were selected to validate the proteomics results, including Mitogen-activated protein kinase kinase kinase kinase 3 (MAP4K3) and Fibrinogen alpha chain (FGA). Both proteins exhibited significant differential expression across four treatment groups (Figure S17). As shown in Figure 6B,C, after exposure to PS@BaP and PS@BaP@BALF MPs, the expression levels of MAP4K3 were significantly down-regulated. MAP4K3 is involved in stress response and may regulate the MAPK and NF-κB signaling pathways. The results suggested that BaP may disrupt the normal regulation of the MAPK/NF-κB pathway, thereby exacerbating inflammatory and toxic responses. And the expression levels of FGA were significantly up-regulated in RAW264.7 cells when exposed to PS @BALF and PS@BaP@BALF MPs. FGA plays a role in inflammation resolution, so its upregulation suggested that it may mitigate MPs-induced cytotoxicity or inflammatory responses by activating tissue repair or inflammation resolution mechanisms. Western blot results were in agreement with proteomics results.

Overall, proteomics results indicated that different MPs affected toxic responses in RAW264.7 cells through multiple signaling pathways, including activation of inflammation, oxidative stress, DNA damage, and phagocytic clearance. These differential mechanisms revealed the underlying mechanisms of the cytotoxic effects of MPs at the protein level, providing new insights.

4. CONCLUSIONS

In this work, we systematically investigated how BaP adsorption (eco-corona) and BALF proteins (biocorona) reshape the physicochemical properties and biological effects of PS MPs. First, corona formation significantly altered the surface characteristics of MPs: BALF coronas increased surface hydrophilicity and reduced surface charge, whereas BaP adsorption altered interfacial charge, thereby influencing the composition and abundance of protein coronas. Second, BALF coronas promoted the cellular uptake of PS MPs by RAW264.7 cells via caveolin-mediated endocytosis, with SP-A identified as a crucial mediator of phagocytosis. Third, BaP adsorption intensified cellular toxicity, oxidative stress, and apoptosis, while BALF coronas exhibited protective effects against membrane damage and apoptosis. It revealed that the BaP corona and BALF corona exerted entirely opposite toxic effects on PS MPs. Interestingly, the elevated oxidative stress associated with BALF coronas may result from enhanced phagocytosis. Finally, proteomics analysis further revealed that corona-coated MPs activated multiple cellular pathways related to inflammation, oxidative damage, DNA damage, and phagocytosis, offering support for the observed cytotoxic effects and contrary actions of two coronas at the mechanistic level. In conclusion, these findings provide new insights into the mechanisms underlying the respiratory toxicity of airborne MPs, and underscore the importance of incorporating both pollutant adsorption and protein corona formation into health risk assessments. However, this study has several limitations that point to key directions for future work: (1) extending the framework to prevalent atmospheric MPs (e.g., polyethylene and polypropylene) at environmentally relevant levels; (2) employing species-matched, and ideally human-relevant, lung multicellular models to clarify biological effects and human health impacts; (3) investigating the dynamics of mixed corona formation and its regulation of cellular uptake and toxicity; (4) developing a standard assay to quantify the "corona modulation factor" of MPs for composite risk assessment.

■ ASSOCIATED CONTENT

Supporting Information

The Supporting Information is available free of charge at https://pubs.acs.org/doi/10.1021/envhealth.5c00747.

Environmental details; particle size distribution of PS, PS@BALF, PS@BaP, and PS@BaP@BALF MPs measured by SEM; element mapping images of PS@BALF MPs; standard calibration curve of BaP; SDS-PAGE analysis of protein coronas formed on MPs; identification of BALF protein; Venn diagram of protein numbers identified on the coronas of PS and PS@BaP MPs; hydrodynamic dimensions of PS, PS@BALF, PS@SP-A MPs; cell viability of RAW264.7 cells after exposure to three endocytic inhibitors, including CPZ, MβCD, and EIPA; cell viability of PS, PS@BALF, PS@BaP, PS@BaP@BALF MPs for 24 h; cell viability of RAW264.7 cells after exposure to BaP for 24 and 48 h; top 30 enriched GO terms in GO analysis of DEPs in RAW264.7 cells after exposure to PS, PS@BALF, PS@

https://doi.org/10.1021/envhealth.5c00747
Environ. Health 2026, 4, 1567−1580

BaP, PS@BaP@BALF MPs; KEGG map of the phagosome pathway in RAW264.7 cells affected by PS@BALF and PS@BaP@BALF MPs for 24 h; fold changes and p values of the DEPs (MAP4K3 and FGA) in RAW264.7 cells affected by PS, PS@BALF, PS@BaP, PS@BaP@BALF MPs; adsorption concentration and rate of BaP-adsorbed PS MPs; main parameters of the searching database in Pro DIA proteomics; composition of proteins identified in the protein corona of PS@BALF and PS@BaP@BALF MPs; DEPs in RAW264.7 cells after exposure to PS, PS@BALF, PS@BaP, PS@BaP@BALF MPs for 24 h (PDF)

AUTHOR INFORMATION

Corresponding Authors

Li Mao − *Ministry of Education (MOE) Key Laboratory of Modern Toxicology, School of Public Health, Nanjing Medical University, Nanjing 211166, China*; Email: maoli@njmu.edu.cn

Hong-zhen Lian − *State Key Laboratory of Analytical Chemistry for Life Science, Jiangsu Key Laboratory of Clean Energy Catalysis and Intelligent Green Chemical Engineering, School of Chemistry & Chemical Engineering and Center of Materials Analysis, Nanjing University, Nanjing 210023, China*; orcid.org/0000-0003-1942-9248; Email: hzlian@nju.edu.cn

Authors

Rui Hou − *State Key Laboratory of Analytical Chemistry for Life Science, Jiangsu Key Laboratory of Clean Energy Catalysis and Intelligent Green Chemical Engineering, School of Chemistry & Chemical Engineering and Center of Materials Analysis, Nanjing University, Nanjing 210023, China*

Ye-xuan Zhang − *State Key Laboratory of Analytical Chemistry for Life Science, Jiangsu Key Laboratory of Clean Energy Catalysis and Intelligent Green Chemical Engineering, School of Chemistry & Chemical Engineering and Center of Materials Analysis, Nanjing University, Nanjing 210023, China*

Si-si Chen − *State Key Laboratory of Analytical Chemistry for Life Science, Jiangsu Key Laboratory of Clean Energy Catalysis and Intelligent Green Chemical Engineering, School of Chemistry & Chemical Engineering and Center of Materials Analysis, Nanjing University, Nanjing 210023, China*

Sen Zhang − *State Key Laboratory of Analytical Chemistry for Life Science, Jiangsu Key Laboratory of Clean Energy Catalysis and Intelligent Green Chemical Engineering, School of Chemistry & Chemical Engineering and Center of Materials Analysis, Nanjing University, Nanjing 210023, China*

Hong-juan Chen − *State Key Laboratory of Pharmaceutical Biotechnology, School of Life Science, Nanjing University, Nanjing 210023, China*

Yong Wang − *State Key Laboratory of Analytical Chemistry for Life Science, Medical School, Nanjing University, Nanjing 210093, China*

Wei-juan Zheng − *State Key Laboratory of Pharmaceutical Biotechnology, School of Life Science, Nanjing University, Nanjing 210023, China*

Hong-wei Wang − *State Key Laboratory of Analytical Chemistry for Life Science, Medical School, Nanjing University, Nanjing 210093, China*; orcid.org/0000-0003-2868-5112

Complete contact information is available at: https://pubs.acs.org/10.1021/envhealth.5c00747

Author Contributions

R.H.: Investigation, Methodology, Formal analysis, Visualization, Writing − original draft. Y.Z.: Investigation, Methodology, Data curation. S.C.: Methodology, Formal analysis. S.Z.: Methodology, Visualization. L.M.: Investigation, Methodology, Funding acquisition, Resources. H.C.: Methodology, Formal analysis. Y.W.: Methodology, Resources. W.Z.: Resources, Validation. H.W.: Investigation, Resources. H.L.: Conceptualization, Methodology, Funding acquisition, Project administration, Writing − review and editing.

Notes

The authors declare no competing financial interest.

ACKNOWLEDGMENTS

This work was supported by the National Natural Science Foundation of China (22176085, 21874065, 91643105).

REFERENCES

(1) Wen, Z.; Xie, Y.; Chen, M.; Dinga, C. D. China's plastic import ban increases prospects of environmental impact mitigation of plastic waste trade flow worldwide. *Nat. Commun.* **2021**, *12* (1), 425.

(2) Thompson, T. Plastic pollution: Three problems that a global treaty could solve. *Nature* **2022**.

(3) Stegmann, P.; Daioglou, V.; Londo, M.; van Vuuren, D. P. P.; Junginger, M. Plastic futures and their CO_2 emissions. *Nature* **2022**, *612* (7939), 272−276.

(4) Cao, J.; Yang, Q.; Jiang, J.; Dalu, T.; Kadushkin, A.; Singh, J.; Fakhrullin, R.; Wang, F.; Cai, X.; Li, R. Coronas of micro/nano plastics: a key determinant in their risk assessments. *Part. Fibre Toxicol.* **2022**, *19* (1), 55.

(5) Andrady, A. L. Microplastics in the marine environment. *Mar. Pollut. Bull.* **2011**, *62* (8), 1596−1605.

(6) Song, Y. K.; Hong, S. H.; Jang, M.; Han, G. M.; Jung, S. W.; Shim, W. J. Combined effects of UV exposure duration and mechanical abrasion on microplastic fragmentation by polymer type. *Environ. Sci. Technol.* **2017**, *51*, 4368.

(7) Koelmans, B.; Pahl, S.; Backhaus, T.; Bessa, F.; van Calster, G.; Contzen, N.; Cronin, R.; Galloway, T.; Hart, A.; Henderson, L., et al. *SAPEA Science Advice for Policy by European Academies. A scientific perspective on microplastics in nature and society*; SAPEA: Berlin, Germany, 2019.

(8) EFSA Panel on Contaminants in the Food Chain (CONTAM). Presence of microplastics and nanoplastics in food, with particular focus on seafood. *Efsa J.* **2016**, *14*(6), e04501. .

(9) Koelmans, A. A.; Redondo-Hasselerharm, P. E.; Nor, N. H. M.; de Ruijter, V. N.; Mintenig, S. M.; Kooi, M. Risk assessment of microplastic particles. *Nat. Rev. Mater.* **2022**, *7* (2), 138−152.

(10) López, A. P. A.; Trilleras, J.; Arana, V. A.; Garcia-Alzate, L. S.; Grande-Tovar, C. D. Atmospheric microplastics: exposure, toxicity, and detrimental health effects. *RSC Adv.* **2023**, *13* (11), 7468−7489.

(11) Hong, R. Y.; Shi, Y. J.; Fan, Z. C.; Gao, Y. J.; Chen, H.; Pan, C. Chronic exposure to polystyrene microplastics induces renal fibrosis via ferroptosis. *Toxicology* **2024**, *509*, 153996.

(12) Leslie, H. A.; van Velzen, M. J. M.; Brandsma, S. H.; Vethaak, A. D.; Garcia-Vallejo, J. J.; Lamoree, M. H. Discovery and quantification of plastic particle pollution in human blood. *Environ. Int.* **2022**, *163*, 107199.

(13) Ragusa, A.; Svelato, A.; Santacroce, C.; Catalano, P.; Notarstefano, V.; Carnevali, O.; Papa, F.; Rongioletti, M. C. A.; Baiocco, F.; Draghi, S.; D'Amore, E.; Rinaldo, D.; Matta, M.; Giorgini, E. Plasticenta: first evidence of microplastics in human placenta. *Environ. Int.* **2021**, *146*, 106274.
(14) Kopatz, V.; Wen, K. V.; Kovács, T.; Keimowitz, A. S.; Pichler, V.; Widder, J.; Vethaak, A. D.; Hollóczki, O.; Kenner, L. Micro- and nanoplastics breach the blood−brain barrier (BBB): biomolecular corona's role revealed. *Nanomaterials* **2023**, *13* (8), 1404.
(15) Sharma, P.; Vidyarthi, V. K. Impact of microplastic intake via poultry products: environmental toxicity and human health. *J. Hazard. Mater. Adv.* **2024**, *14*, 100426.
(16) Saenen, N. D. Redox-mediated toxicity of micro- and nanoplastics in intestinal models. *Toxicol. Lett.* **2024**, *399*, S16.
(17) Cortés, C.; Domenech, J.; Salazar, M.; Pastor, S.; Marcos, R.; Hernández, A. Nanoplastics as a potential environmental health factor: effects of polystyrene nanoparticles on human intestinal epithelial Caco-2 cells. *Environ. Sci.: Nano* **2020**, *7* (1), 272−285.
(18) Qiu, L.; Lu, W. F.; Tu, C. L.; Li, X. L.; Zhang, H.; Wang, S. G.; Chen, M. Z.; Zheng, X. B.; Wang, Z. G.; Lin, M. M.; Zhang, Y. M.; Zhong, C. H.; Li, S. F.; Liu, Y. W.; Liu, J.; Zhou, Y. Evidence of microplastics in bronchoalveolar lavage fluid among never-smokers: a prospective case series. *Environ. Sci. Technol.* **2023**, *57* (6), 2435−2444.
(19) Huang, S. M.; Huang, X. X.; Bi, R.; Guo, Q. X.; Yu, X. L.; Zeng, Q. H.; Huang, Z. Y.; Liu, T. M.; Wu, H. S.; Chen, Y. L.; Xu, J. L.; Wu, Y. G.; Guo, P. Detection and analysis of microplastics in human sputum. *Environ. Sci. Technol.* **2022**, *56* (4), 2476−2486.
(20) Lu, W. F.; Li, X. L.; Wang, S. G.; Tu, C. L.; Qiu, L.; Zhang, H.; Zhong, C. H.; Li, S. F.; Liu, Y. W.; Liu, J.; Zhou, Y. New evidence of microplastics in the lower respiratory tract: inhalation through smoking. *Environ. Sci. Technol.* **2023**, *57* (23), 8496−8505.
(21) Baeza-Martinez, C.; Olmos, S.; Gonzalez-Pleiter, M.; Lopez-Castellanos, J.; Garcia-Pachon, E.; Masia-Canuto, M.; Hernandez-Blasco, L.; Bayo, J. First evidence of microplastics isolated in European citizens' lower airway. *J. Hazard. Mater.* **2022**, *438*, 129439.
(22) Amato-Lourenço, L. F.; Carvalho-Oliveira, R.; Ribeiro, G.; Galvao, L. D.; Ando, R. A.; Mauad, T. Presence of airborne microplastics in human lung tissue. *J. Hazard. Mater* **2021**, *416*, 126124.
(23) Sun, A. Q.; Wang, W. X. Human exposure to microplastics and its associated health risks. *Environ. Health* **2023**, *1* (3), 139−149.
(24) Dong, C. D.; Chen, C. W.; Chen, Y. C.; Chen, H. H.; Lee, J. S.; Lin, C. H. Polystyrene microplastic particles: in vitro pulmonary toxicity assessment. *J. Hazard. Mater.* **2020**, *385*, 121575.
(25) Cao, J. W.; Xu, R.; Geng, Y.; Xu, S. W.; Guo, M. Y. Exposure to polystyrene microplastics triggers lung injury via targeting toll-like receptor 2 and activation of the NF-KB signal in mice. *Environ. Pollut.* **2023**, *320*, 121068.
(26) Xu, D. H.; Ma, Y. H.; Han, X. D.; Chen, Y. B. Systematic toxicity evaluation of polystyrene nanoplastics on mice and molecular mechanism investigation about their internalization into Caco-2 cells. *J. Hazard. Mater.* **2021**, *417*, 126092.
(27) Yu, Y. N.; Luan, Y. N.; Dai, W. Time evolution of protein corona formed by polystyrene nanoplastics and urease. *Int. J. Biol. Macromol.* **2022**, *218*, 72−81.
(28) Galloway, T. S.; Cole, M.; Lewis, C. Interactions of microplastic debris throughout the marine ecosystem. *Nat. Ecol. Evol.* **2017**, *1* (5), 0116.
(29) Lundqvist, M.; Stigler, J.; Cedervall, T.; Berggård, T.; Flanagan, M. B.; Lynch, I.; Elia, G.; Dawson, K. The evolution of the protein corona around nanoparticles: a test study. *ACS Nano* **2011**, *5* (9), 7503−7509.
(30) Nel, A. E.; Mädler, L.; Velegol, D.; Xia, T.; Hoek, E. M. V.; Somasundaran, P.; Klaessig, F.; Castranova, V.; Thompson, M. Understanding biophysicochemical interactions at the nano-bio interface. *Nat. Mater.* **2009**, *8* (7), 543−557.
(31) Zhang, C.; Lin, X. X.; Gao, P. P.; Zhao, X.; Ma, C. C.; Wang, L.; Sun, H. W.; Sun, L.; Liu, C. G. Combined effects of microplastics and excess boron on Microcystis aeruginosa. *Sci. Total Environ.* **2023**, *891*, 164298.
(32) Zhang, Y. T.; Chen, M. Y.; He, S. Q.; Fang, C.; Chen, M. L.; Li, D.; Wu, D.; Chernick, M.; Hinton, D. E.; Bo, J.; Xie, L. T.; Mu, J. L. Microplastics decrease the toxicity of triphenyl phosphate (TPhP) in the marine medaka (*Oryzias melastigma*) Larvae. *Sci. Total Environ.* **2021**, *763*, 143040.
(33) Mamtimin, X.; Song, W.; Wang, Y.; Habibul, N. Arsenic adsorption by carboxylate and amino modified polystyrene micro- and nanoplastics: kinetics and mechanisms. *Environ. Sci. Pollut. Res.* **2023**, *30* (15), 44878−44892.
(34) Sun, Q.; Lu, F. H.; Ni, H. G. Microplastic-water partitioning of two states halogenated PAHs: solute and sol. *Environ. Res.* **2021**, *202*, 111634.
(35) Moncrieffe, R.; Masry, M.; Cai, B. B.; Rossignol, S.; Kamari, A.; Poirier, L.; Bertrand, S.; Wong-Wah-Chung, P.; Zalouk-Vergnoux, A. Study of the ageing and the sorption of polyaromatic hydrocarbons as influencing factors on the effects of microplastics on blue mussel. *Aquat. Toxicol.* **2023**, *262*, 106669.
(36) IARC Working Group on the Evaluation of Carcinogenic Risks to Humans. Some non-heterocyclic polycyclic aromatic hydrocarbons and some related exposures. *IARC Monogr. Eval. Carcinog. Risks Hum.* **2010**, *92*, 1−853.
(37) Feng, H.; Liu, Y. J.; Xu, Y.; Li, S. X.; Liu, X.; Dai, Y. H.; Zhao, J.; Yue, T. T. Benzo[a]pyrene and heavy metal ion adsorption on nanoplastics regulated by humic acid: Cooperation/competition mechanisms revealed by molecular dynamics simulations. *J. Hazard. Mater.* **2022**, *424*, 127431.
(38) González-Soto, N.; Hatfield, J.; Katsumiti, A.; Duroudier, N.; Lacave, J. M.; Bilbao, E.; Orbea, A.; Navarro, E.; Cajaraville, M. P. Impacts of dietary exposure to different sized polystyrene microplastics alone and with sorbed benzo[*a*]pyrene on biomarkers and whole organism responses in mussels Mytilus galloprovincialis. *Sci. Total Environ.* **2019**, *684*, 548−566.
(39) von Hellfeld, R.; Zarzuelo, M.; Zaldibar, B.; Cajaraville, M. P.; Orbea, A. Accumulation, depuration, and biological effects of polystyrene microplastic spheres and adsorbed cadmium and benzo(*a*)pyrene on the mussel Mytilus galloprovincialis. *Toxics* **2022**, *10* (1), 18.
(40) Xu, Y. W.; Zhu, J.; Hu, J. Y.; Zhang, Z.; Li, L.; Wu, Q. Co-exposure to different sized polystyrene microplastics and benzo[*a*]-pyrene affected inflammation in zebrafish and bronchial-associated cells. *Chin. Sci. Bull.* **2020**, *65* (36), 4281−4290.
(41) Ji, Y. X.; Wang, Y. Q.; Shen, D. H.; Kang, Q.; Chen, L. X. Mucin corona delays intracellular trafficking and alleviates cytotoxicity of nanoplastic-benzopyrene combined contaminant. *J. Hazard. Mater.* **2021**, *406*, 124306.
(42) Bai, X.; Lam, S. M.; Nie, P. C.; Xu, M.; Liu, S. J.; Shui, G. H.; Hu, G. Q. Lipidomic analysis probes lipid coronas on hydrophilic nanoparticles from natural lung surfactant. *Environ. Sci.: Nano* **2022**, *9* (11), 4150−4161.
(43) Yin, B. H.; Chan, C. K. W.; Liu, S. R.; Hong, H. L.; Wong, S. H. D.; Lee, L. K. C.; Ho, L. W. C.; Zhang, L.; Leung, K. C. F.; Choi, P. C.-L.; Bian, L. M.; Tian, X. Y.; Chan, M. N.; Choi, C. H. J. Intrapulmonary cellular-level distribution of inhaled nanoparticles with defined functional groups and its correlations with protein corona and inflammatory response. *ACS Nano* **2019**, *13* (12), 14048−14069.
(44) Poulsen, K. M.; Albright, M. C.; Niemuth, N. J.; Tighe, R. M.; Payne, C. K. Interaction of TiO_2 nanoparticles with lung fluid proteins and the resulting macrophage inflammatory response. *Environ. Sci.: Nano* **2023**, *10* (9), 2427−2436.
(45) Xia, L.; Alqahtani, S.; Ferreira, C. R.; Aryal, U. K.; Biggs, K.; Shannahan, J. H. Modulation of pulmonary toxicity in metabolic syndrome due to variations in iron oxide nanoparticle-biocorona composition. *Nanomaterials* **2022**, *12* (12), 2022.
(46) Shaw, C. A.; Mortimer, G. M.; Deng, Z. J.; Carter, E. S.; Connell, S. P.; Miller, M. R.; Duffin, R.; Newby, D. E.; Hadoke, P. W. F.; Minchin, R. F. Protein corona formation in bronchoalveolar fluid

enhances diesel exhaust nanoparticle uptake and pro-inflammatory responses in macrophages. *Nanotoxicology* **2016**, *10* (7), 981−991.
(47) Whitwell, H.; Mackay, R. M.; Elgy, C.; Morgan, C.; Griffiths, M.; Clark, H.; Skipp, P.; Madsen, J. Nanoparticles in the lung and their protein corona: the few proteins that count. *Nanotoxicology* **2016**, *10* (9), 1385−1394.
(48) Du, T. T.; Yu, X.; Shao, S.; Li, T.; Xu, S. M.; Wu, L. J. Aging of nanoplastics significantly affects protein corona composition thus enhancing macrophage uptake. *Environ. Sci. Technol.* **2023**, *57* (8), 3206−3217.
(49) Liu, W.; Xiong, J. X.; Lai, W. J.; Zhao, H. J.; Peng, D. H.; Zheng, X.; Liao, C. H.; Li, M. J.; Zhang, F.; Wei, J. H.; Wang, J.; Chen, C.; Cai, J.; Zhu, J. P. Microplastics and nanoplastics in indoor environments: Current knowledge and future research. *J. Build. Eng.* **2025**, *114*, 114242.
(50) Choudhury, A.; Simnani, F. Z.; Singh, D.; Patel, P.; Sinha, A.; Nandi, A.; Ghosh, A.; Saha, U.; Kumari, K.; Jaganathan, S. K.; Kaushik, N. K.; Panda, P. K.; Suar, M.; Verma, S. K. Atmospheric microplastic and nanoplastic: The toxicological paradigm on the cellular system. *Ecotoxicol. Environ. Saf.* **2023**, *259*, 115018.
(51) Le, V. G.; Nguyen, M. K.; Nguyen, H. L.; Lin, C.; Hadi, M.; Hung, N. T. Q.; Hoang, H. G.; Nguyen, K. N.; Tran, H. T.; Hou, D.; Zhang, T.; Bolan, N. S. A comprehensive review of micro- and nanoplastics in the atmosphere: Occurrence, fate, toxicity, and strategies for risk reduction. *Sci. Total Environ.* **2023**, *904*, 166649.
(52) Konduru, N. V.; Velasco-Alzate, K.; Adduri, S.; Zagorovsky, K.; Diaz-Diestra, D.; Fisol, F.; Sanches, M.; Ndetan, H.; Brain, J. D.; Molina, R. M. Pulmonary fate and consequences of transferrin-functionalized gold nanoparticles. *Nanotheranostics* **2021**, *5* (3), 309−320.
(53) Wen, J.; Sun, H.; Liu, Z. X.; Zhu, X. Y.; Qin, Z. M.; Song, E. R.; Song, Y. Aging processes dramatically alter the protein corona constitution, cellular internalization, and cytotoxicity of polystyrene nanoplastics. *Environ. Sci. Technol. Lett.* **2022**, *9* (11), 962−968.
(54) Chen, S. S.; Zhang, Y. X.; Chen, H. J.; Zheng, W. J.; Hu, X.; Mao, L.; Guo, X. W.; Lian, H. Z. Surface property and in vitro toxicity effect of insoluble particles given by protein corona: implication for PM cytotoxicity assessment. *Eco-Environ. Health* **2024**, *3* (2), 137−144.
(55) Tan, Y.; Zhu, X. Y.; Wu, D.; Song, E. Q.; Song, Y. Compromised autophagic effect of polystyrene nanoplastics mediated by protein corona was recovered after lysosomal degradation of corona. *Environ. Sci. Technol.* **2020**, *54* (18), 11485−11493.
(56) Khoshnamvand, M.; Hamidian, A. H.; Ashtiani, S.; Ali, J.; Pei, D. S. Combined toxic effects of polystyrene nanoplastics and lead on Chlorella vulgaris growth, membrane lipid peroxidation, antioxidant capacity, and morphological alterations. *Environ. Sci. Pollut. Res.* **2024**, *31* (19), 28620−28631.
(57) Sharma, M. D.; Elanjickal, A. I.; Mankar, J. S.; Krupadam, R. J. Assessment of cancer risk of microplastics enriched with polycyclic aromatic hydrocarbon. *J. Hazard. Mater.* **2020**, *398*, 122994.
(58) Zhou, Q. H.; Wang, L. X.; Cao, Z. Y.; Zhou, X. H.; Yang, F.; Fu, P. Q.; Wang, Z. H.; Hu, J. T.; Ding, L.; Jiang, W. Dispersion of atmospheric fine particulate matters in simulated lung fluid and their effects on model cell membranes. *Sci. Total Environ.* **2016**, *542*, 36−43.
(59) Ghazaryan, A.; Landfester, K.; Mailaender, V. Protein deglycosylation can drastically affect the cellular uptake. *Nanoscale* **2019**, *11* (22), 10727−10737.
(60) Johnston, B. D.; Kreyling, W. G.; Pfeiffer, C.; Schäffler, M.; Sarioglu, H.; Ristig, S.; Hirn, S.; Haberl, N.; Thalhammer, S.; Hauck, S. M.; et al. Colloidal stability and surface chemistry are key factors for the composition of the protein corona of inorganic gold nanoparticles. *Adv. Funct. Mater.* **2017**, *27* (42), 1701956.
(61) McKenzie, Z.; Kendall, M.; Mackay, R. M.; Whitwell, H.; Elgy, C.; Ding, P.; Mahajan, S.; Morgan, C.; Griffiths, M.; Clark, H.; Madsen, J. Surfactant protein A (SP-A) inhibits agglomeration and macrophage uptake of toxic amine modified nanoparticles. *Nanotoxicology* **2015**, *9* (8), 952−962.
(62) Doumanov, J.; Jordanova, A.; Zlatkov, K.; Moskova-Doumanova, V.; Lalchev, Z. Investigation of IL-6 effects on SP-A expression in A549 lung cell line. *Biotechnol. Biotechnol. Equip.* **2012**, *26*, 96−99.
(63) Chen, J.; Xu, Z. J.; Liu, Y. Y.; Mei, A. X.; Wang, X. Y.; Shi, Q. D. Cellular absorption of polystyrene nanoplastics with different surface functionalization and the toxicity to RAW264.7 macrophage cells. *Ecotoxicol. Environ. Saf.* **2023**, *252*, 114574.
(64) Hou, Y. S.; Tu, S. Y.; Zhao, X. H.; Li, G. Y.; Li, N.; Zou, A. H. An integrative method for evaluating the biological effects of nanoparticle-protein corona. *Biochim. Biophys. Acta BBA* **2023**, *1867* (3), 130300.
(65) Raesch, S. S.; Tenzer, S.; Storck, W.; Rurainski, A.; Selzer, D.; Ruge, C. A.; Perez-Gil, J.; Schaefer, U. F.; Lehr, C. M. Proteomic and lipidomic analysis of nanoparticle corona upon contact with lung surfactant reveals differences in protein, but not lipid composition. *ACS Nano* **2015**, *9* (12), 11872−11885.
(66) McCormack, F. X.; Festa, A. L.; Andrews, R. P.; Linke, M.; Walzer, P. D. The carbohydrate recognition domain of surfactant protein a mediates binding to the major surface glycoprotein of pneumocystis carinii. *Biochemistry* **1997**, *36* (26), 8092−8099.
(67) Sever-Chroneos, Z.; Krupa, A.; Davis, J.; Hasan, M.; Yang, C. H.; Szeliga, J.; Herrmann, M.; Hussain, M.; Geisbrecht, B. V.; Kobzik, L.; Chroneos, Z. C. Surfactant protein A (SP-A)-mediated clearance of staphylococcus aureus involves binding of SP-A to the Staphylococcal Adhesin Eap and the macrophage receptors SP-A receptor 210 and scavenger receptor class A. *J. Biol. Chem.* **2011**, *286* (6), 4854−4870.
(68) Huang, W. T.; Yin, H.; Yang, Y. Y.; Jin, L. Z.; Lu, G. N.; Dang, Z. Influence of the co-exposure of microplastics and tetrabromobisphenol A on human gut: simulation in vitro with human cell Caco2 and gut microbiota. *Sci. Total Environ.* **2021**, *778*, 146264.
(69) Li, Z. K.; Zhu, S. X.; Liu, Q.; Wei, J. L.; Jin, Y. C.; Wang, X. F.; Zhang, L. S. Polystyrene microplastics cause cardiac fibrosis by activating Wnt/β-catenin signaling pathway and promoting cardiomyocyte apoptosis in rats. *Environ. Pollut.* **2020**, *265*, 115025.
(70) Su, K. J.; Jin, X. T.; Zhang, W. F.; Li, Z. Y.; Liu, X. N.; Ren, J. Particulate matter exposure induces the autophagy of macrophages via oxidative stress-mediated PI3K/AKT/mTOR pathway. *Chemosphere* **2017**, *167*, 444−453.
(71) Finaud, J.; Lac, G.; Filaire, E. Oxidative stress - relationship with exercise and training. *Sports Med.* **2006**, *36* (4), 327−358.
(72) Xue, D. H.; Huang, J. N.; Sun, X.; Zhang, W.; Ma, H.; Yin, D.; Wang, Y. H.; Wang, J. G.; Yang, C. B.; Geng, Q. S. Dissection of the potential mechanism of polystyrene microplastic exposure on cardiomyocytes. *Sci. Total Environ.* **2025**, *973*, 179048.
(73) Wen, J. H.; Li, D. Y.; Liang, S.; Yang, C.; Tang, J. X.; Liu, H. F. Macrophage autophagy in macrophage polarization, chronic inflammation and organ fibrosis. *Front. Immunol.* **2022**, *13*, 946832.
(74) Fang, L.; Wu, H. M.; Ding, P. S.; Liu, R. Y. TLR2 mediates phagocytosis and autophagy through JNK signaling pathway in staphylococcus aureus-stimulated RAW264.7 cells. *Cell. Signalling* **2014**, *26* (4), 806−814.
(75) Wang, X.; Guillem-Marti, J.; Kumar, S.; Lee, D. S.; Cabrerizo-Aguado, D.; Werther, R.; Alamo, K. A. E.; Zhao, Y. T.; Nguyen, A.; Kopyeva, I.; et al. De novo design of integrin $\alpha5\beta1$ modulating proteins to enhance biomaterial properties. *Adv. Mater.* **2025**, *37* (34), 2500872.
(76) Sarkar, J.; Wen, X.; Simanian, E. J.; Paine, M. L. V-type ATPase proton pumpexpression during enamel formation. *Matrix Biol.* **2016**, *52*−*54*, 234−245.
(77) Zhang, C. S.; Jiang, B.; Li, M.; Zhu, M.; Peng, Y.; Zhang, Y. L.; Wu, Y.-Q.; Li, T. Y.; Liang, Y.; Lu, Z.; et al. The lysosomal v-ATPase-regulator complex is a common activator for AMPK and mTORC1, acting as a switch between catabolism and anabolism. *Cell Metab.* **2014**, *20* (3), 526−540.
(78) Fu, B.; Ye, X.; Zhou, Y.; Che, J.; Huang, W.; Chen, J. Personal exposure to microplastics and PAHs in $PM_{2.5}$: Personal vs. outdoor assessment and health risks. *J. Hazard. Mater.* **2025**, *496*, 139249.

https://doi.org/10.1021/envhealth.5c00747
Environ. Health 2026, 4, 1567−1580